Journal of *Marine Science and Engineering*

MDPI

Article

Morphodynamic Response of Open and Embayed Beaches to Winter Conditions: Two Case Studies from the North Atlantic Iberian Coast

Ángela Fontán-Bouzas [1,*], Tiago Abreu [2], Caroline C. Ferreira [3,4], Paulo A. Silva [5], Laura López-Olmedilla [5], José Guitián [1], Ana M. Bernabeu [1] and Javier Alcántara-Carrió [6]

1 Centro de Investigación Mariña, Universidade de Vigo, GEOMA, 36310 Vigo, Spain; jose.guitian@uvigo.gal (J.G.) bernabeu@uvigo.gal (A.M.B.)
2 CESAM, ISEP, Polytechnic of Porto, 4249-015 Porto, Portugal; taa@isep.ipp.pt
3 Observatório Oceânico da Madeira, Agência Regional para o Desenvolvimento da Investigação, Tecnologia e Inovação (ARDITI), 9020-105 Funchal, Portugal; caroline.ferreira@oom.arditi.pt
4 Laboratório Associado Instituto Dom Luiz (IDL), Faculdade de Ciências, Universidade de Lisboa, 1749-016 Lisboa, Portugal
5 CESAM, Department of Physics, University of Aveiro, 3810-193 Aveiro, Portugal; psilva@ua.pt (P.A.S.); lauraolmedilla@ua.pt (L.L.-O.)
6 Department of Geology and Geochemistry, Faculty of Sciences, Autonomous University of Madrid, 29049 Madrid, Spain; javier.alcantara@uam.es
* Correspondence: afontan@uvigo.gal

Abstract: The morphological responses of two mesotidal beaches located in different coastal settings (embayed and open sandy beaches) on the northwestern Iberian coast were monitored during the winter of 2018/19. The offshore wave time series analysis is related to high-resolution topo-bathymetric measurements to explore spatial-temporal morphological variability at monthly to seasonal scales. Both locations are subjected to the North Atlantic wave climate which exhibits a pronounced seasonality. Throughout the last decade (2010–2020), significant wave heights reached values of up to H_s~9 m during winters and up to H_s~6 m during summers. On average, approximately 12 storms occurred annually in this region. The results clearly reveal divergent morphological responses and sediment transport behaviors at the upper beach and the intertidal zone during the winter for each location. In the embayed beach (Patos), sediment transport in the nearshore is governed by cross-shore processes between the beach berm and a submerged sandbar. In contrast, the open beach (Mira) showed dynamic sediment exchanges and three-dimensional morphologies alternating between accumulation and erosion zones. Overall, both beaches exhibited an erosional trend after the winter, particularly concerning berm erosion and the subaerial beach volume/shoreline retreat. This study highlights the contrasting morphodynamic response on open and embayed beaches to winter conditions, integrating both the subaerial and submerged zones. Local geological and environmental factors, as well as the coastal management strategies applied, will influence how the beach responds to winter wave events. Monitoring and understanding these responses are essential for effective coastal management and adaptation to changing climate.

Keywords: beach survey; nearshore; morphological changes; bathymetry; extreme events

Citation: Fontán-Bouzas, Á.; Abreu, T.; C. Ferreira, C.; Silva, P.A.; López-Olmedilla, L.; Guitián, J.; Bernabeu, A.M.; Alcántara-Carrió, J. Morphodynamic Response of Open and Embayed Beaches to Winter Conditions: Two Case Studies from the North Atlantic Iberian Coast. *J. Mar. Sci. Eng.* **2024**, *12*, 168. https://doi.org/10.3390/jmse12010168

Academic Editor: Eugen Rusu

Received: 10 December 2023
Revised: 9 January 2024
Accepted: 10 January 2024
Published: 15 January 2024

1. Introduction

Beaches are naturally dynamic sandy systems where morphological changes are primarily associated with the variability of incident wave energy, eroding and accreting in response to changing wave conditions [1,2]. Beaches subjected to high wave energy can experience intensive erosion, making them vulnerable zones for coastal ecosystems. Additionally, in the context of climate change, other factors need to be considered as

significant threats to beach systems, such as sediment deficit, sea-level rise, population growth, and litter pollution [3–5].

In high wave energy environments, morphodynamic changes in the subaerial and intertidal zones of the beaches have been extensively described, while changes in the submerged zone are generally less studied due to limited bathymetric data and challenges to monitoring them. Changes in beach bathymetry are closely linked to subaerial morphology, as they are controlled by nearshore processes. Submerged features, such as nearshore bars, play a crucial role as large sediment reservoirs, dissipating incoming wave energy and significantly affecting the coast, particularly during storm events [6]. Therefore, understanding transport processes in the submerged zone is essential for a complete morphodynamic modeling of coastal regions.

Coastal impacts on beaches during winter seasons have been globally studied in recent decades [7–11]. However, assessing wave responses in specific areas remains necessary, as the morphodynamic response of a beach can vary significantly due to site-specific conditions, such as beach type and local geology, which are influenced by regional geological and oceanographic processes [9,12]. Sandy coasts exposed to energetic waves are particularly vulnerable to winter storms, which can induce dramatic morphological changes, exacerbated by potential climate change scenarios [13]. Therefore, local investigations are needed to address and model these future changes [14].

The northwest coast of the Iberian Peninsula, exposed to the Atlantic Ocean fetch, experiences a strongly seasonal wave regime, peaking in winter [15], with a highly variability in the occurrence of storms. Most of the storms affecting the European Atlantic coasts originate in the mid-latitude westerly wind belt [16]. Storminess in the Atlantic is strongly linked to the North Atlantic Oscillation [17] and the West Europe Pressure Anomaly (WEPA; [18]), characterized by considerable inter-annual and inter-decadal variability. Recent research has examined whether winter conditions may have intensified in recent decades over northern Europe [19,20]. However, uncertainties remain regarding the characteristics of winter waves and their consequences in the NW Iberia coastal system in the context of climate change.

Morphological characteristics and exposure to specific hydrodynamic conditions define how beaches are prone to wave-induced coastal erosion [21,22]. Therefore, studies of individual beaches contribute to our understanding and generalization of beach morphodynamics [23], and accurate beach field observations help to uncover and understand their behavior. Various geological contexts define the beach configurations analyzed in this study, including open sandy beaches and sheltered or embayed (pocket) beaches. On open sandy beaches, severe erosion is traditionally associated with single [9] or consecutive extreme storms [24,25]. In contrast, pocket or embayed beaches are constrained sedimentary systems influenced by sediment availability and accommodation space [26–28]. Shorelines of embayed beaches can remain relatively stable over longer time periods, with seasonal beach cycles strongly associated with wave variability at seasonal and event-driven time scales [29].

The main objective of this study is to compare the morphodynamic response of an open beach and an embayed beach under the same winter wave conditions, both for the emerged and submerged zones. To attain this goal, the specific objectives are: (i) to characterize and compare the wave forcing, i.e., the wave storm conditions affecting both study sites, and (ii) to investigate the morphological response of both beaches during winters. Two sandy beaches with contrasting geological features have been chosen from the NW northwestern Iberian coast. Detailed analyses of similarities or differences in both hydrodynamic forcing and concurrent winter-driven morphological changes in the subaerial and submerged zones of both beaches during winter 2018/19 have been carried out. Changes in the shoreline position, presence of berms and submerged bars, and beach sediment volumes have been analyzed.

2. Regional Setting and Study Areas

The northwestern Iberian coastal zone is characterized by a wide variety of beach morphologies. The linear sandy coastline of Portugal contrasts with the intricate coastline on the Spanish side. The Portuguese coastline consists of open, wave-dominated beaches with extensive dune fields in the hinterland. The Spanish coast comprises several drowned valleys (estuaries of the rias subtype) with interspersed pocket beaches. In this study, we selected two study areas in the northwestern Iberian coast, approximately 200 km apart Patos and Mira beaches (Figure 1 and Table 1).

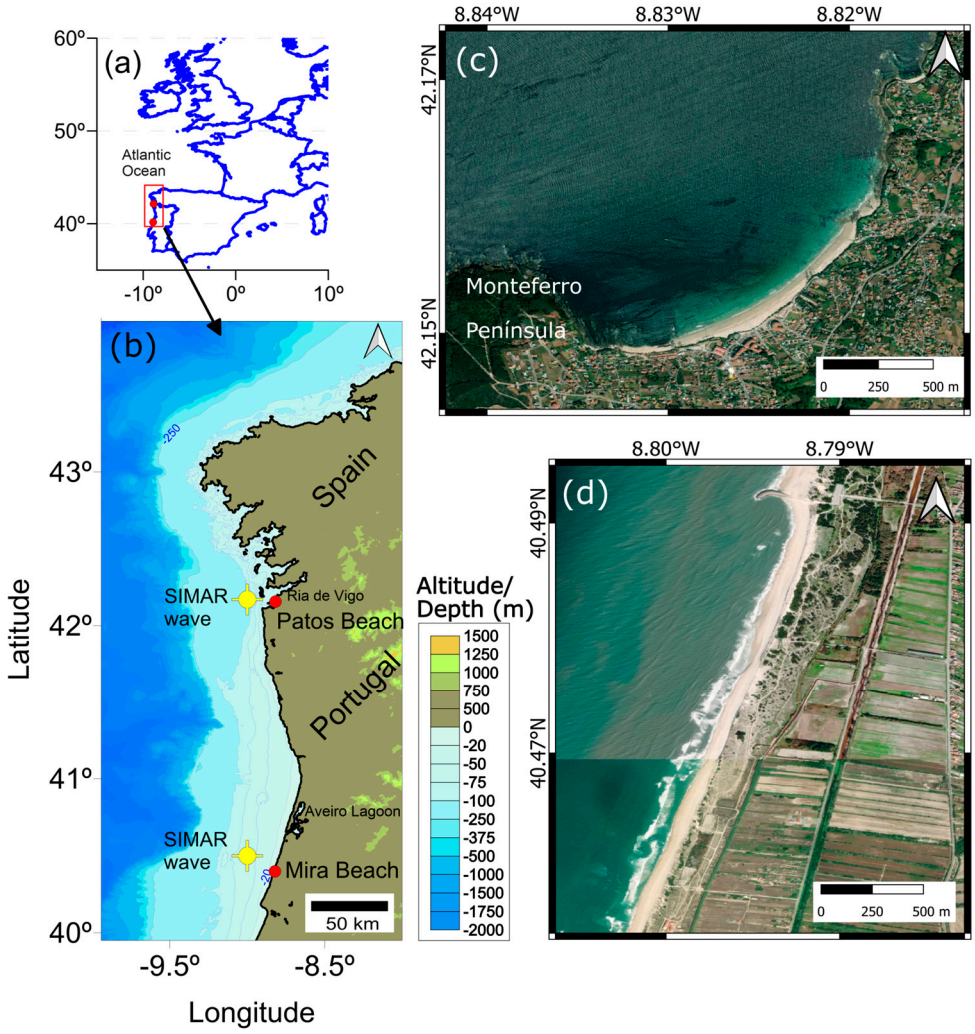

Figure 1. Geographical setting of the study area: (**a**) location of the NW Iberian Region, (**b**) location of the study sites (red dots) and SIMAR wave points (yellow dots) on the NW Iberian Peninsula, (**c**) Patos Beach, (**d**) Mira Beach.

Patos Beach (42°09′18.80″ N, 8°49′33.05″ W) is an embayed/pocket beach bordered on the west by the Monteferro Peninsula, located on the southern margin of the outer sector of the Ria de Vigo drowned valley, in northwestern Spain. The beach is 1200 m long and nearly 70 m width. The shoreline is oriented ENE-WSW and features rocky outcrops at both ends [30,31]. It can be considered an urban beach, bounded by a promenade and buildings. The most frequent directions of offshore wave are NW-WNW, varying throughout the year [32]. The beach undergoes seasonal equilibrium, with sediments being removed during winter and replaced in summer, resulting in a wide berm and a moderate slope of the beach face [33]. The sediment size corresponds to fine sand, with a median grain size

(D_{50}) of approximately 0.236 mm [32]. The local tide is mesotidal and semidiurnal, with a mean range of 2.2 m [30]

Table 1. Morpho-sedimentary characteristics of Patos and Mira beaches: type, D_{50}, slope, width, berm height above mean sea level, based on [30,34].

Beach	Type	D_{50} (mm)	Beach Slope (°)	Beach Width (m)	Berm Height (m)
Patos	Embayed	0.2–0.3	0.02–0.07	70–100	3–4
Mira	Open	0.4–0.6	0.05–0.15	40–80	3–5

Mira Beach (40°27′28.76″ N, 8°48′10.74″ W) is an open sandy beach located on the north-central Portuguese coast (Figure 1). The beach has a length of 2500 m and an average width varying from about 40 to 80 m, as observed during the winter 2016/17 [34]. The beach is oriented NNE-SSW, limited to the north by a 200 m long groin and backed by a dune system with crest elevations ranging from 5 to 16 m. This study site is part of a sandy barrier system, bounded to the east by the Aveiro lagoon. The dune system behind Mira Beach serves as a geomorphological element of protection for various socio-economic activities located eastward of these dunes. The beach is composed of medium sand (D_{50}~0.4 mm) that is supplied by a natural N-S littoral drift [35–37]. A long-term erosional trend has been ongoing in this coastal stretch, influenced by a deficit of sediment supply from the Douro River, which decreased from 1.5 million m³/year to about 0.25 million m³/year over the last decades [38–40]. Due to the severe erosion trends in this coastal stretch, the Portuguese National Environmental Agency (APA) conducted dune nourishments mainly to the north of this sector, coast of Aveiro region [41]. The tidal regime is semidiurnal mesotidal, with an average amplitude of 2.20 m, reaching a maximum elevation of 4 m during spring tides [42].

3. Methods

The dataset investigated in the present study comprises hourly hydrodynamic data series (2010–2020) and a collection of topographical and bathymetric surveys (all acquired between September 2018 and June 2019).

3.1. Offshore Hydrodynamic Data

The offshore hydrodynamic data were obtained from SIMAR Points refs: 3012004 and 1044062, provided by Puertos del Estado (https://www.puertos.es/ (accessed on 14 December 2022), location in Figure 1). The SIMAR dataset comprises synthetic time series of wind and wave parameters generated using the WAM and WaveWatch models, driven by the wind fields from the HIRLAM model [43]. Both WAM and WaveWatch models are third-generation spectral models that solve the energy balance equation without making any a priori assumptions about the shape of the wave spectrum. The first modeled wave node (9.00° E, 42.17° N) is located about 8 km northwest of Patos Beach at a depth of 95 m, while the other modeled wave node (9.00° E, 40.50° N) is 75 m deep and 18.5 km offshore of Mira Beach. The SIMAR dataset provides hourly hydrodynamic data from 1958 to the present. This study analyzes the hydrodynamic data of the last decade (2010–2020) for both locations, focusing on the dates of field surveys carried out between September 2018 and June 2019.

A storm event is defined following the approach initially proposed by [44] when significant wave height (Hs) exceeds 4 m ($H_{95\%}$) during a complete tidal cycle, which corresponds to a 12 h period. A cluster or sequence of storms is defined as a succession of two or more storms if the calm period between events is shorter than five days [45].

According to the linear approach, the wave energy flux towards the coast, denoted as P_{tot}, is given by

$$P_{tot} = \frac{1}{8}\rho g H_s^2 C_g, \quad (1)$$

where ρ represents the density of ocean water (1025 kg/m^3), g is the gravitational acceleration (9.81 m/s^2) and C_g is the wave group velocity defined by Equation (2):

$$C_g = \frac{1}{2}c\left(1 + \frac{2kd}{sinh(2kd)}\right), \quad (2)$$

where C is the phase velocity (Equation (3)),

$$C = \sqrt{\frac{g}{k}tanh(kd)} \quad (3)$$

where, k is the wavenumber and d is the depth. The wavenumber k has been calculated by solving the linear dispersion relation.

3.2. Field Surveys (Data Collection) and Processing

Two beaches on the northwest Iberian coast were selected as part of a regional monitoring program initiated in 2016. For this research, the topography of the subaerial and intertidal coastal sites was measured simultaneously between September 2018 and June 2019, using a Trimble real-time kinematic global positioning system (RTK_DGPS) on foot (see Table 2). In Mira Beach, the analysis focused on the cross-shore transect below mean sea level (MSL), and the dune was surveyed during the same periods (Figure 2). Bathymetric measurements at Patos were carried on a vessel with Multibeam Sonar both pre- and post-winter conditions using a multibeam echosounder (MBES- Kongsberg GS+ equipment) were position was determined by GPS with RTK corrections and system calibrated at each survey for positioning delay, roll, pitch and heading deviation yielding a precision within 0.4 m depth at fixed points. The topo-bathymetric data at Mira Beach was provided by the Portuguese Coastal Monitoring Program—COSMO at https://cosmo.apambiente.pt (accessed on 17 June 2022). Therefore, in addition to the DGPS surveys on the subaerial beach, a total of 4 bathymetric maps were obtained, one for pre-winter and another one for post-winter 2018/19 at each location (2 MBES dataset for Patos, and 2 COSMO dataset for Mira).

Figure 2. Images showing the RTK_DGPS beach profiles (black dashed lines) and topo bathymetric survey areas (marked in green) in Patos (**left**) and Mira (**right**) beaches.

Table 2. Field measurement dataset over the study period and vertical accuracy, root mean square error (RMSE).

Patos Beach	Mira Beach	Measurement	RMSE (m)
	1 September 2018	Topo-bathy COSMO	0.3
21 September 2018	28 September 2018	Topo-bathy MBES	0.4
22 October 2018	22 October 2018	DGPS	0.05
8 November 2018	1 November 2018	DGPS	0.05
21 December 2018	21 December 2018	DGPS	0.05
11 January 2019	15 January 2019	DGPS	0.05
4 February 2019	4 February 2019	DGPS	0.05
22 May 2019	22 May 2019	DGPS	0.05
22 May 2019	-	Topo-bathy MBES	0.4
	19 June 2019	Topo-bathy COSMO	0.3

Table 2 summarizes the monitoring techniques used in this study for both sites. The beach profiles were carefully chosen in representative areas of each study site. At Patos Beach, the profile was extracted from location away from the direct influence of the rocky headlands. At Mira Beach, the selected profile is located far enough from the northernmost groin (Figure 2).

To determine the winter variability in beach morphology, three-dimensional topographic beach surface maps were analyzed. Two primary beach erosion indicators were extracted based on the measured cross-shore profiles: the shoreline position and beach volume. The shoreline isocontour was identified at MSL positions corresponding to the elevation $z = 0$ according to the ETRS89 vertical datum. The beach volume (m^3/m) of the active subaerial zone is defined as the area delimited between a landward position with no vertical variation and the seaward limit established by the MSL. Therefore, it was integrated from the measured cross-shore profiles (see dates in Table 2)

4. Results

4.1. Decadal Wave Hydrodynamics

An overview of the offshore wave characteristics over the past decade (2010–2020), separated by winter and summer seasons, is provided in Tables 3 and 4 for the Patos and Mira beaches, respectively. There is a strong agreement in mean values between the wave parameters for both locations, since the data follow the one-to-one correspondence shown in the dashed lines of Figure 3. This high correlation in offshore hydrodynamic data can be justified by the relatively short distance between both SIMAR points, slightly more than 200 km (Figure 1b).

Additionally, noticeable seasonality in wave conditions is observed for both locations. During the winter, typically from October to March, the mean significant wave height (H_s~2.5 m) is generally associated with longer wave peak periods (T_p~12.3 s). In contrast, during the summer, from April to September, much weaker conditions (H_s~1.6 m) prevail, associated with shorter wave periods (T_p~9.8 s). These differences are also reflected in wave energies and energy fluxes, according to Equation (1). During the summer, the mean energy for both locations is lower than 5×10^3 J/m^2. However, during the winter, the average mean energy is about twice as high as the summer values (~9.5×10^3 J/m^2). The differences between summer and winter are also evident in the total energy fluxes, with the winter values representing more than three times the values during the summer.

The most energetic winters in the dataset are 2013/14, 2015/16 and the last three winters of the decade (2017/18, 2018/19, and 2019/2020). The winter 2018/19, during which the field surveys were conducted, reflects a typical energetic winter at both locations.

Table 3. Patos offshore wave regime: significant wave heights (H_s), wave peak periods (T_p), wave group velocity (C_g), wave energy and wave energy fluxes, and mean wave steepness. In bold are the winters where the mean energy values exceed the threshold of 9.5×10^3 J/m².

		H_s Max (m)	H_s Mean (m)	T_p Max (s)	T_p Mean (s)	C_g Max (m/s)	Mean Energy (J/m^2) $\times 10^3$	Total Energy Flux (W/m) $\times 10^8$	Mean Wave Steep.
Summer	2010	6.6	1.4	18.2	9.6	16.9	3.1	1.2	0.009
Winter	2010/11	6.9	2.0	19.5	11.7	18.3	6.4	3.1	0.009
Summer	2011	5.5	1.4	19.6	9.7	18.4	2.9	1.2	0.009
Winter	2011/12	6.2	2.0	20.5	12.2	19.1	6.1	2.9	0.009
Summer	2012	4.6	1.5	19.3	9.4	18.1	3.3	1.2	0.011
Winter	2012/13	6.7	2.6	18.4	12.1	17.2	**9.9**	4.5	0.011
Summer	2013	5.6	1.5	19.5	9.6	18.2	3.6	1.4	0.010
Winter	2013/14	8.5	2.9	20.5	12.9	19.1	**13.5**	7.2	0.011
Summer	2014	5.6	1.5	19.1	9.4	17.8	3.3	1.3	0.010
Winter	2014/15	6.0	2.3	20.9	12.4	19.5	7.5	3.7	0.009
Summer	2015	4.7	1.6	19.0	9.8	17.8	3.8	1.5	0.010
Winter	2015/16	7.0	2.7	20.2	12.2	18.9	**10.6**	5.1	0.012
Summer	2016	4.6	1.5	17.7	10.0	16.4	3.2	1.3	0.009
Winter	2016/17	8.9	2.0	18.8	11.8	17.5	6.8	3.3	0.009
Summer	2017	4.9	1.5	17.2	9.9	15.9	3.4	1.3	0.010
Winter	2017/18	8.9	2.7	21.5	12.4	20.0	**10.9**	5.4	0.011
Summer	2018	4.8	1.5	19.5	10.8	18.3	3.4	1.4	0.008
Winter	2018/19	8.3	2.7	21.5	12.8	20.0	**10.7**	5.4	0.011
Summer	2019	4.4	1.7	21.5	9.8	20.0	4.1	1.5	0.011
Winter	2019/20	9.7	2.9	21.5	12.6	20.0	**12.6**	6.3	0.012

Table 4. Mira offshore wave regime: significant wave heights (H_s), wave peak periods (T_p), wave group velocity (C_g), wave energy and wave energy fluxes, and mean wave steepness. In bold are the winters where the mean energy values exceed the threshold of 9.5×10^3 J/m^2.

		H_s Max (m)	H_s Mean (m)	T_p Max (s)	T_p Mean (s)	C_g Max (m/s)	Mean Energy (J/m²) $\times 10^3$	Total Energy Flux (W/m) $\times 10^8$	Mean Wave Steep.
Summer	2010	6.6	1.7	18.2	9.5	17.0	4.3	1.6	0.012
Winter	2010/11	7.9	2.1	19.7	11.6	18.2	6.9	3.4	0.010
Summer	2011	5.2	1.7	19.4	9.6	18.0	4.1	1.6	0.011
Winter	2011/12	5.6	2.1	20.7	12.1	18.9	6.5	3.2	0.009
Summer	2012	4.0	1.6	18.8	9.5	17.5	3.7	1.3	0.011
Winter	2012/13	10.3	2.7	19.0	12.1	17.7	**10.4**	5.0	0.012
Summer	2013	4.9	1.7	20.6	9.6	18.8	4.5	1.7	0.012
Winter	2013/14	7.7	2.9	20.7	12.9	18.9	**12.8**	7.1	0.012
Summer	2014	5.0	1.6	19.3	9.6	17.9	3.8	1.5	0.011
Winter	2014/15	5.7	2.4	21.0	12.4	19.1	8.7	4.3	0.010
Summer	2015	4.6	1.7	19.5	9.9	18.1	4.4	1.7	0.011

Table 4. *Cont.*

		H_s Max (m)	H_s Mean (m)	T_p Max (s)	T_p Mean (s)	C_g Max (m/s)	Mean Energy (J/m²) ×10³	Total Energy Flux (W/m) ×10⁸	Mean Wave Steep.
Winter	2015/16	7.0	2.7	20.8	12.2	19.0	**10.5**	5.3	0.012
Summer	2016	4.6	1.7	17.6	10.0	16.5	4.0	1.6	0.011
Winter	2016/17	7.8	2.1	19.0	11.9	17.7	7.0	3.5	0.010
Summer	2017	4.5	1.7	16.3	9.9	15.2	4.0	1.6	0.011
Winter	2017/18	8.7	2.8	21.5	12.6	19.4	**12.2**	6.5	0.012
Summer	2018	4.8	1.6	21.5	10.8	19.4	4.0	1.7	0.009
Winter	2018/19	8.8	2.6	21.5	12.8	19.4	**9.8**	5.2	0.010
Summer	2019	3.8	1.7	21.5	9.7	19.4	4.2	1.6	0.011
Winter	2019/20	7.7	2.7	21.5	12.8	19.4	**10.6**	5.6	0.011

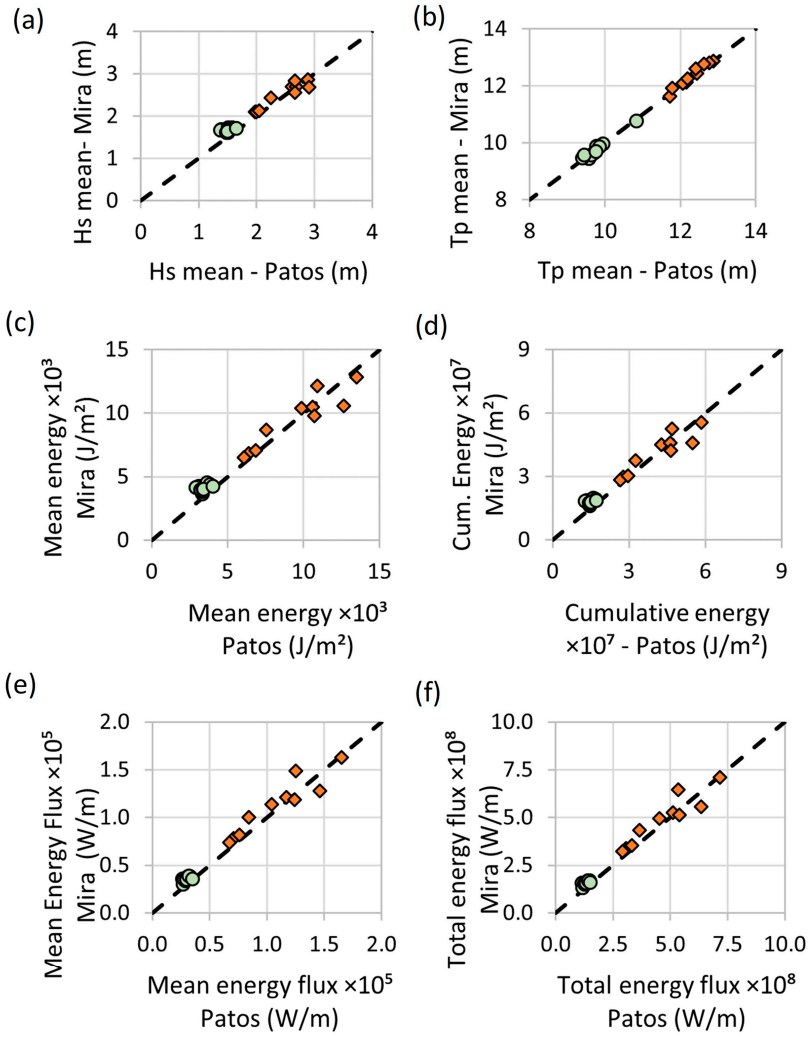

Figure 3. Winter (diamonds) and summer (circles) wave characteristics for Mira and Patos: (**a**) mean significant wave height (**b**) mean peak periods (**c**) mean wave energy, (**d**) cumulative wave energy, (**e**) mean wave energy fluxes and (**f**) total wave energy fluxes.

The storm activity for both locations exhibit an average of 12 storms per year, ranging from 5 to 22 at Patos and 5 to 23 at Mira (Figure 4). In agreement with the previous results

regarding total energy fluxes, the longest storm duration is observed during the 2013/14 winter, with a total storm duration of 918 h at Patos and 801 h at Mira. This represents more than twice the total storm duration compared to the other years. The number of storm clusters per year varies between one and five at both locations. The amount of storms within clusters ranges from a minimum of two storms to a maximum of nine storms, which occurred during the winter of 2017/18 at Mira. During the severe 2013/14 winter, four clusters were identified at Patos: two of them included seven storm sequences, one included three storm sequences, and another included two storm sequences. For Mira, three clusters were identified: two of them included six storm sequences, and another included three storm sequences.

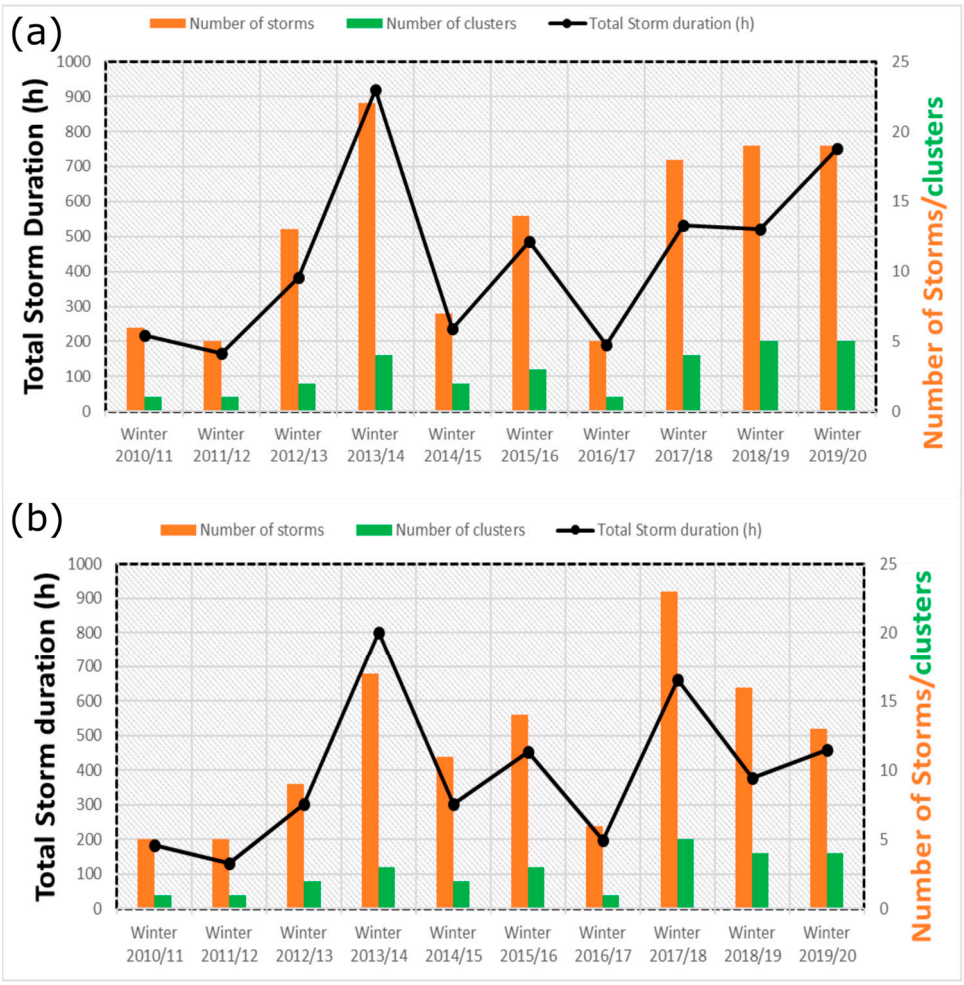

Figure 4. Winter storm characteristics for (**a**) Patos and (**b**) Mira: total storm duration (black), number of storms (orange), and number of storm clusters (green).

Interestingly, the total storm duration during the 2018/19 winter is about half that of the 2013/14 winter, despite having a similar number of storms and clusters. In 2018/19 (2013/14), 19 (22) storms and 5 (4) groups were observed at Patos, while 16 (17) storms and 4 (3) clusters were observed at Mira. Despite this apparent similarity, the mean storm duration between both years is quite different, as reflected in the energy results in the previous section. In winters of 2013/14 and 2018/19, the mean storm duration was 42 and 27 h at Patos, and 47 and 24 h at Mira, respectively.

4.2. Wave Hydrodynamics of Winter 2018/19

The variations in H_s, T_p, and mean wave direction (θ_m) over time exhibit similar patterns for both locations, despite minor differences (Figure 5). Overall, the early winter

period from November to mid-December is characterized by high energy conditions, and energetic storms with maximum H_s values occurred in February. Some periods of lower energy were also observed, such as from the 21 December to the 30 January and from 7 to 21 March 2019.

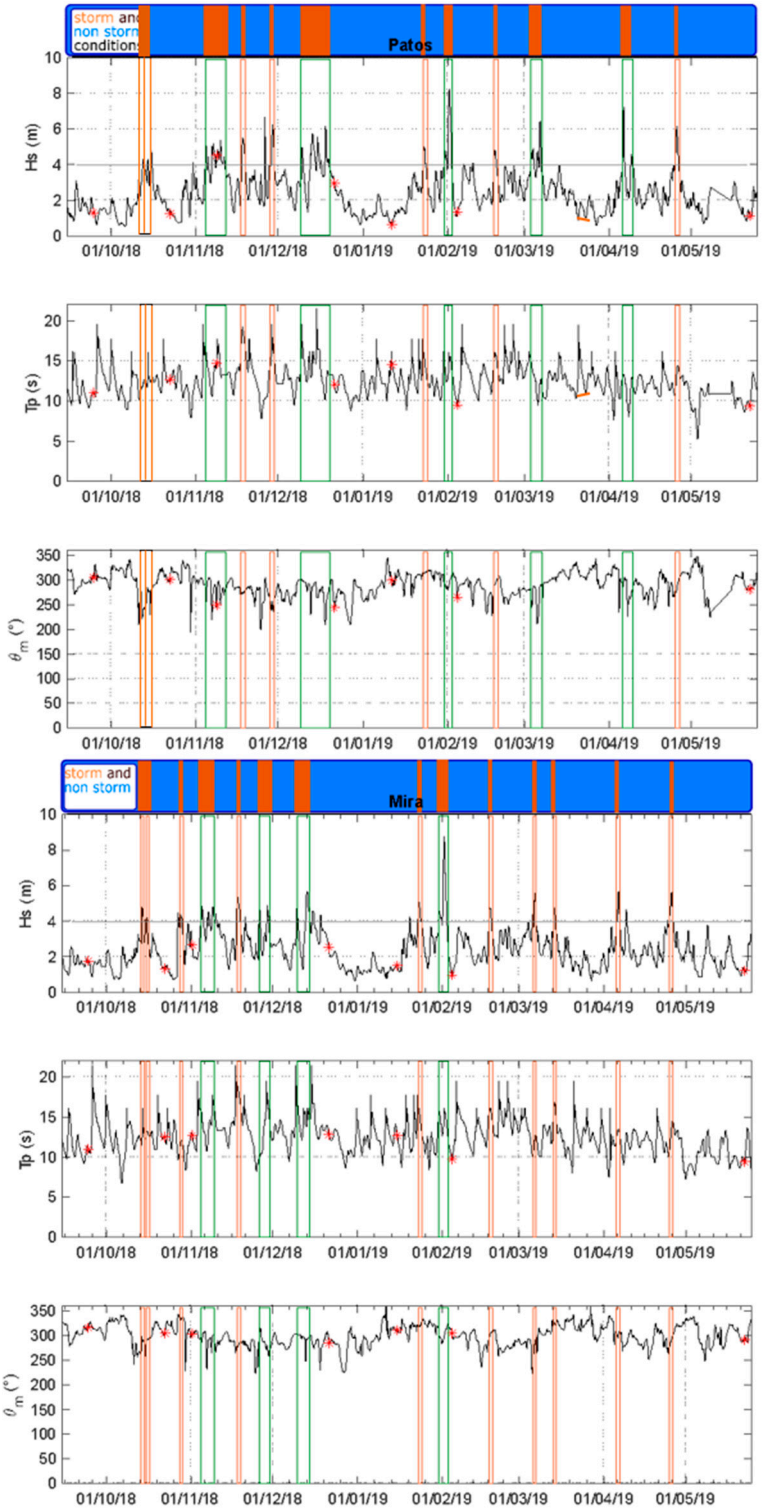

Figure 5. Hydrodynamic conditions (Hs, Tp, and θm) at Patos (**above**) and Mira (**below**). Red stars represent the surveys, and the orange and green lines mark individual storms and storm clusters, respectively. Orange and blue sections in the top timeline box identifies storm and non-storm conditions, respectively.

Patos beach is characterized by the occurrence of 19 individual storms with an average duration of 27 h, slightly lower than the average over the last decade (34 h). The longest storm lasted 75 h, beginning on the 8 November 2018. The highest H_s value (8.29 m) was recorded on the 1 February 2019. In the case of Mira, 16 individual storms were identified, with an average duration of 24 h, and the longest storm lasted up to 38 h, starting on the 13 December 2018. Similarly, for Patos, the highest H_s value (8.79 m) was observed on the 1st of February; considering storm sequencing, five clusters are observed (Figure 5). Two sequences include two storms (from 30 January 2019 to 2 February 2019 and from 5 April 2019 to 9 April 2019), two sequences with three storms (from 4 November 2018 to 11 November 2018 and from 3 March 2019 to 7 March 2019), and one sequence of four storms (from 9 December 2018 to 19 December 2018). For Mira, 16 individual storms are identified with an average duration of 24 h, also slightly lower than the average over the last decade (32 h). Accounting for storm sequencing, four clusters can be observed: three sequences of two storms (from 25 November 2018 to 29 November 2018, from 9 December 2018 to 14 December 2018, and from 30 January 2019 to 2 February 2019) and one sequence of three storms (from 4 November 2018 to 9 November 2018).

The wave regime at both sites is primarily characterized by H_s, following a Rayleigh distribution, where lower H_s values have a higher frequency than greater H_s values. In the interval (2–3) m, relative frequencies are close to 34%, and between (1–2) m relative frequencies are around 30%. Approximately 12% of the data correspond to $H_s > 4$ m, which therefore is defined as the threshold for quantifying storms and storm sequences in this region.

The majority of T_p values fall within the range of (12–14) s, with relative frequencies of 48%, followed by the intervals (10–12) s and (14–16) s, with relative frequencies of about 20% and 15%, respectively.

There is a predominance of wave directions in the range of (292.5–360) degrees, accounting for approximately 36% of occurrences. However, the main directions for Patos are in the interval (292.5–315) degrees, representing about 16% of occurrences, whereas for Mira, it is in the interval (337.5–360) degrees, accounting for approximately 18% of the data.

4.3. Topo-Bathymetric Changes

The accuracy of the topographic dataset (MBES+DGPS and COSMO for Patos and Mira, respectively) allowed us to compute beach topo-bathymetric DEMs with meter resolution at pre- and post-winter states. These surface maps cover from the upper part of the beach (up to 6 m above mean sea level) to the submerged proximal area (until 20 m deep), including therefore the nearshore, and upper and lower shoreface. Subsequently, differences between DEMs were calculated (Figures 6 and 7).

The beach and subtidal zones of Patos exhibit a relatively uniform longitudinal morphology, with consistent contours from the subaerial beach to the deeper zones. The subaerial beach features a berm morphology positioned above 2.5 m (above MSL). The subtidal shoreface has a gentle slope with a gradual increase in depth from the upper subtidal to the deeper zone. The rocky outcrops at both edges of the beach result in some irregularities in the DEM contours, while the regular slope in the central zone is rather associated with a sandy bed level. A significant morphological change is observed between fall 2018 and spring 2019 (Figure 6). The beach experienced a negative net sediment budget (i.e., erosion) during the survey period, highlighting erosion exceeding 1 m at the beach berm. In contrast, accretion is observed after winter on the submerged subtidal shoreface, particularly between the -1 and -4 m contours, demonstrated by a newly formed sandbar at -2 m depth approximately 150 m away from the shoreline.

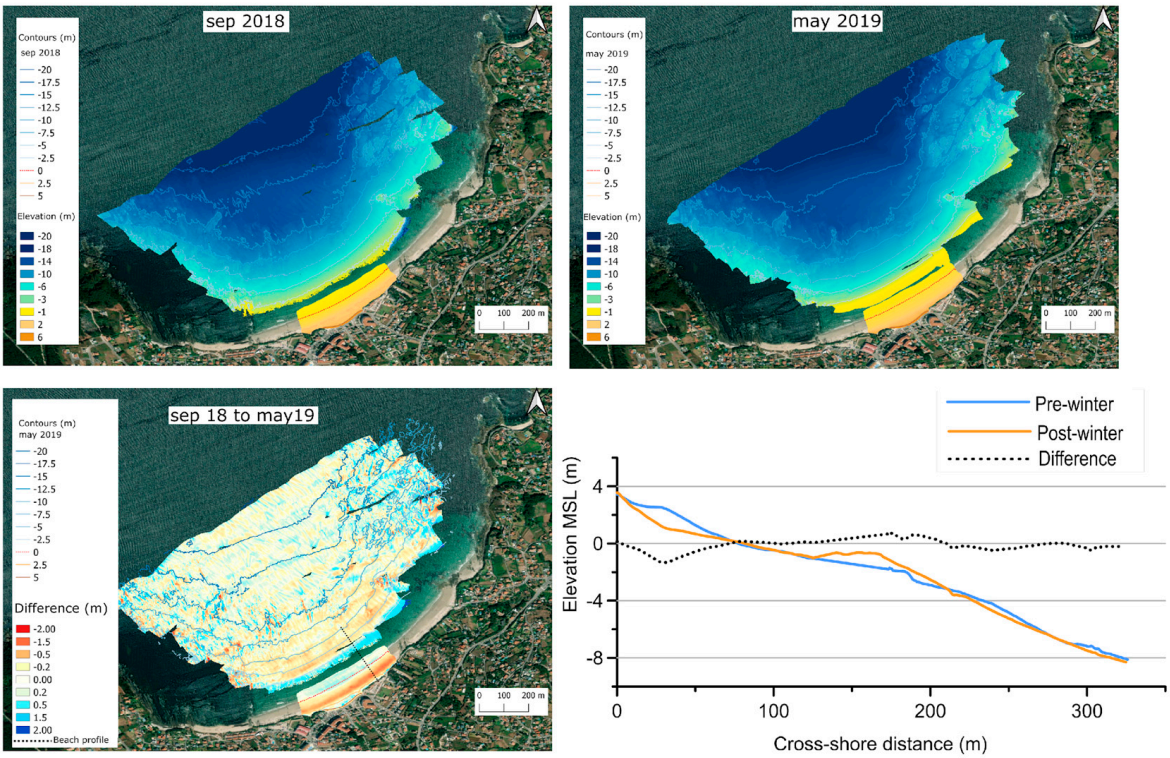

Figure 6. Morphologic beach changes at Patos due to winter wave conditions of 2018/19. The top panels show the pre-winter (September 2018) and post-winter (May 2019) topo-bathymetric maps (DEMs, altitudes above MSL). The bottom-left panel shows the maps of differences in altitude, with positive and negative values for accretion and erosion, respectively. The bottom-right panel displays two subaerial and subtidal cross-shore profiles for the representative site (see location in the bottom-left panel), for the pre-winter (blue line) and post-winter (orange line) morphologies, and the differences in elevation (dashed black line) between them, again with positive and negative values for accretion and erosion, respectively.

On the other hand, the beach and subtidal areas at Mira Beach exhibit a complex three-dimensional morphology with shifting morphological features. The changes of the berm position and the sandbar shape imply a highly dynamic environment. For instance, berm's height depends on the location varies along the beach, reaching over 4 m MSL in the southern part, where the selected profile is located, due to higher dunes back up. In the submerged zone, sandbars are visible from -1 to -5 m deep. Thus, there is significant alongshore variability and changeable beach morphologies noted from the north to the southern beach sections in Mira. The largest morphological change during the winter of 2018/19 is found at Mira in the subtidal zone, near the sandbar morphologies reaching almost 4 m, and also at berm features on the subaerial beach, demonstrated by vertical variations exceeding ± 1.5 m (Figure 7 and Figure S1 of the Supplementary Material). The Supplementary Figure S1 for Mira displays four additional topo-bathymetric profiles 500 m apart for the pre- and post-winter surfaces, as well as the differences in cross-shore elevation between them. At these submerged beach profiles the morphological changes reach up to 2 m. The volume of sand involves greatest variability in alongshore change occurred in the submerged zone at Mira Beach, being more variable than the emerged beach, where significant morphologic changes also occur.

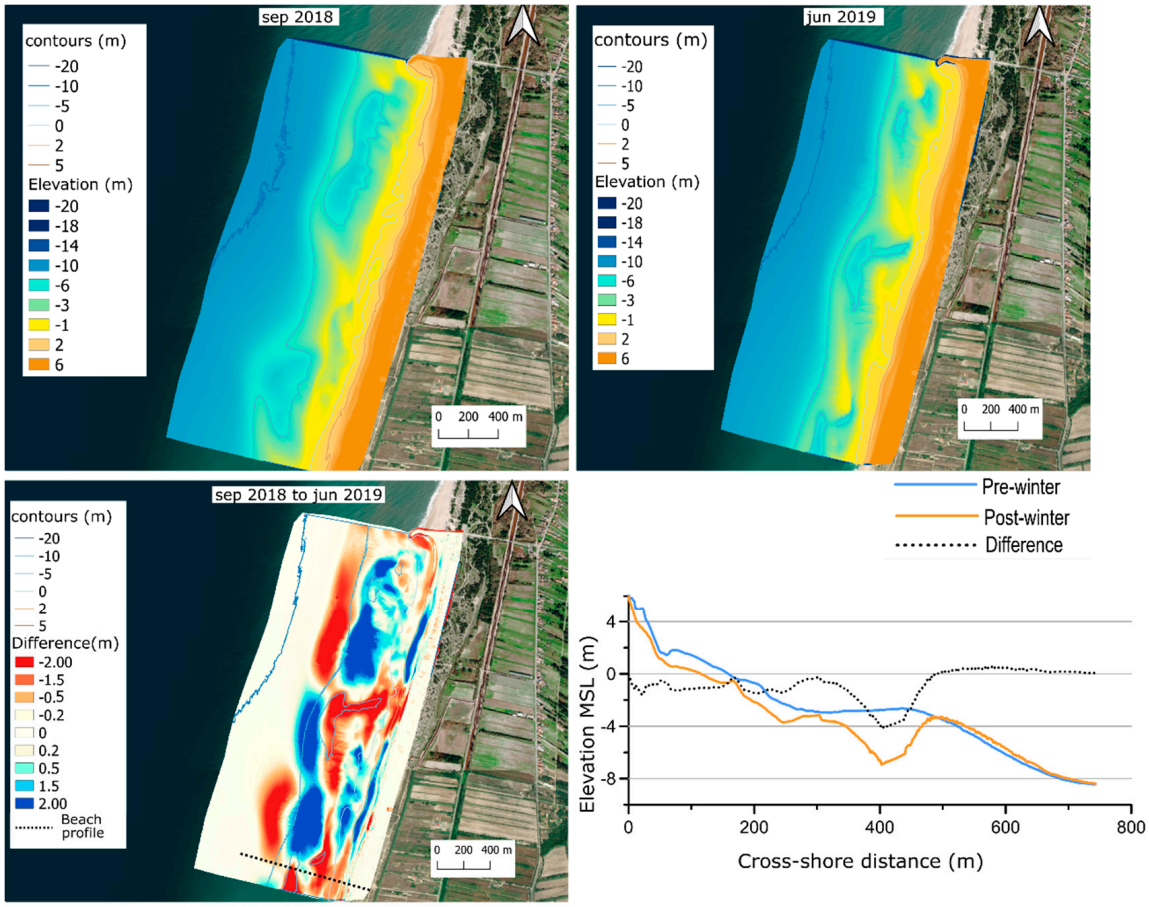

Figure 7. Morphologic beach changes at Mira due to winter wave conditions of 2018/19. The top panels show the Pre-winter (September 2018) and post-winter (May 2019) topo-bathymetric maps (DEMs, altitudes above MSL). The bottom-left panel shows the maps of elevation differences in altitude, with positive and negative values for accretion and erosion, respectively. The bottom-right panel displays two subaerial and subtidal cross-shore profiles for the representative site (see location in the bottom-left panel), with blue, orange, and black dashed lines for the pre-winter, (blue line) and post-winter (orange line) morphologies, and the differences in elevation (dashed black line) between them, again with positive and negative values for accretion and erosion, respectively.

From the DEM comparison (bottom-left panels of Figures 6 and 7), it is possible to identify the depth of closure, i.e., the cross-shore distance where morphological changes can be considered insignificant. The observed depth of closure in this period (September 2018 to June 2019) is about −8 m for Patos (Figure 6) and is deeper for Mira, at approximately −9.5 m deep (Figure 7 and Figure S1 of the Supplementary Material). Both beaches show erosion of the beach berm. Subaerial sediments were removed or partially transferred to the submerged area. Overall, the sediment budget for Patos Beach is −0.16 m^3/m^2 (−18,049.92 m^3 for a planar area of 116,209.21 m^2). In contrast, the sediment budget for Mira Beach is 0.09 m^3/m^2 (160,374.33 m^3 for a planar area of 1,816,983.88 m^2).

4.4. Beach Profile Response to Winter 2018/19

Patos and Mira beaches exhibit well-defined berm features before the winter period (in September 2018). After the first storms in November and mid-December, a significant reduction in the berm is observed. Winter conditions, with the occurrence of storms, promote morphological changes, being erosion characterized by changes in the berm height and shoreline positions, and a smoothing of the beach slope. In the case of Mira Beach, the berm partially recovers after experiencing mild conditions in January 2019, but is later removed during the second energetic period in February 2019. In Patos, the berm is eroded

throughout the winter, but shows a slight recovery trend in the spring of 2019. The sediment volume of the supratidal beach is reduced, especially at Mira Beach (Figure 8).

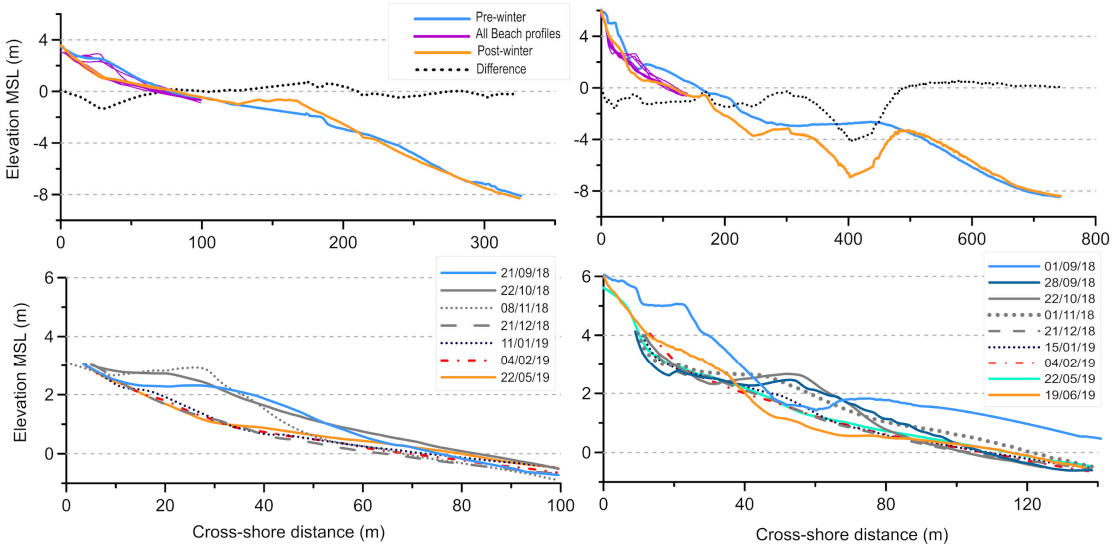

Figure 8. Temporal evolution of beach profiles of Patos (**left panels**) and Mira (**right panels**) throughout winter 2018/19. In the top panels, the dataset includes all topobathymetric and subaerial profiles. The bottom panels detail the subaerial beach, with pre-winter (blue lines), monthly measurements (colors-dashed lines), and post-winter (orange lines).

Beach erosion was generally the dominant process. Both beaches partially recovered some sediments under the mild wave conditions during January, showing an increase in the volume of sand in the subaerial beach. However, the storms that induced the most significant impacts with remarkable vertical and horizontal variations did not coincide (Figure 9).

In September 2018, the profile volume at Patos Beach exceeded 100 m^3/m and then gradually decreased throughout the winter. The beach lost sediment abruptly between November and December during the longest winter storm period, including storm sequences in November and December. The beach profile reduced suddenly by 50 m^3/m, with a shoreline landward displacement of −12 m. For the rest of the surveyed period, the initial position of the shoreline was recovered, but, all together, the beach profiles eroded up to 40 m^3/m, corresponding to a 40% loss of the subaerial beach volume.

Mira's volume was initially 230 m^3/m and was reduced to 190 m^3/m after the initial storms in November. Subsequently, at the end of January, the beach profile recovered, gaining sediments up to 265 m^3/m. The greatest erosion impacts were observed with the February storm, corresponding to the most intense storm of the winter with the highest significant wave height (8.79 m). The beach volume was reduced by up to 170 m^3/m, and the shoreline retreated up to −44 m from its initial position.

After February, during the final study period, which extended through 22 May 2019, both study sites exhibited a differentiated wave-induced response. Patos showed an incipient sediment recovery, while Mira beach profile showed an erosion trend, losing more than 50% of the initial subaerial beach volume. The data also indicate that the shoreline response is highly variable, and its migration correlates well with the volume of sand involved. However, during the mild period between December 2018 and January 2019, the shoreline migration and volume at Mira were negatively correlated.

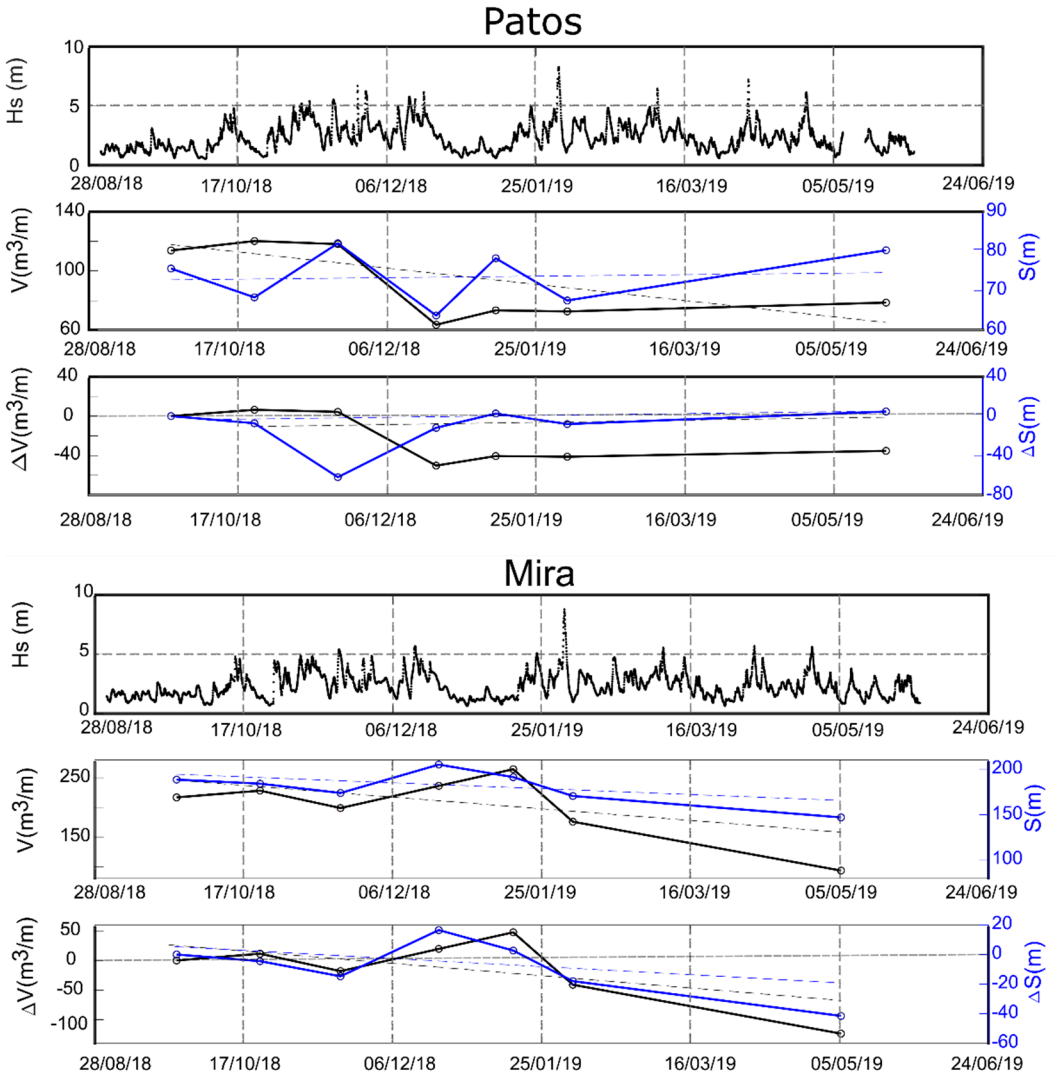

Figure 9. Significant wave height versus vertical and horizontal erosion indicators: beach volume (black line), shoreline positions (blue line), beach volume and shoreline changes throughout the winter and Linear trends (dashed black, blue lines) for Patos and Mira.

5. Discussion

The results presented in this study allow to explore the hydrodynamics and morphological response to winter conditions of an embayed/pocket beach and an open sandy beach located in the NW Iberian coast. Different morphological responses were observed despite similarities in the incident wave regime and tide conditions.

5.1. Wave Forcing

Similarities in offshore wave conditions are described for both locations (Section 4.1). Energetic waves prevail during the winter (H_s~2.5 m, T_p~12.3 s), while weaker conditions occur from May to October (H_s~1.6 m, T_p~9.8 s). The main wave direction for both study sites is in the interval 270−360°, showing a slight trend of northernmost at Mira. This implies a pronounced seasonality of wave forcing, consistent with previous research in nearby Atlantic latitudes (e.g., Biscarrosse Beach, SW France [45]. When considering the decadal analysis, the results highlight winters 2013/14 and 2017/18 as the most energetic ones. This observation aligns with previous studies that documented significant damage along the European coasts during these energetic winters [46–49]. Additionally, previous analysis of wave datasets along the Portuguese mainland coast under storm conditions over almost three decades (1988–2015) described winter of 2013/14 as the one with more

in situ storms recorded on the Portuguese West coast [50]. In particular, December 2013 to February 2014 was the period with the highest number of consecutive storms at the Leixões buoy (located about 100 km apart of Patos and Mira, in between) [51,52], which is in agreement with our results.

The most energetic winters within the decade are 2012/13, 2013/14, 2015/16 and the last three winters 2017/18, 2018/19 and 2019/2020. In comparison, the 2018/19 winter was less energetic than 2013/14, but significant storms and storm clusters occurred and are analyzed with the morphological dataset of this research. The wave parameters, number of storms per year and winter sequences in NW Iberian had not been quantified before to the best of the authors' knowledge. Wave characteristics and storm frequency could also be related to the variability of climate indices, e.g., NAO or WEPA [18]. Although a causality of the NAO is beyond the scope of this research, it is worth mentioning that previous studies have already established relationships between coastal morphological changes and NAO phases for other Atlantic coasts of Europe [53].

5.2. Beach Response to Winter Conditions

The analysis of the morphological data considered in this study shows a large variability in the beach response at the two locations, despite the similarities in the wave forcing. Therefore, in this section we aim to identify and define the main drivers of beach morphology based on our obtained dataset.

When comparing the morphological responses of the Patos embayed beach and the open sandy Mira Beach, major changes are observed in Mira, with higher vertical variations exceeding ±2 m and significant alongshore and cross-shore variability (Table 5). At Mira Beach there is a contrasting behavior between the northern and southern stretches, in agreement with the previous monitoring in winter 2016/17 [34], is observed also the gradual formation and disappearance of the beach berm in the intertidal area. In contrast, Patos Beach exhibits less variability, a gradual response along the subaerial and submerged beach and a relatively uniform longitudinal morphology. At Patos Beach, the sediment from the aerial beach feeds the nearby submerged zone in winter, developing a submerged sandbar. The extracted nearshore profiles indicate the disappearance of the beach berm at both beaches after the winter 2018/19. Sediment transport at Patos Beach is predominantly cross-shore, in agreement with previous research [33,54].

Table 5. Summary of morphological changes in the embayed Patos Beach and the open Mira Beach under the same wave conditions in winter 2018/19.

	Shoreline Position	**Beach Slope**	**Berm Height**	**Submerged Bars**	**Subaerial Volume Changes**	**Sediment Transport**
Embayed Patos Beach	Quasi stable	Gradual decrease and uniform alongshore	Gradual decrease	Development of only 1 bar	Low erosional trend	Mainly cross-shore
Open Mira Beach	More dynamic (retreat)	Rapid changes and variable alongshore	Abrupt decrease	Migration of several bars	High erosional trend	Long-shore and cross-shore

Therefore, our results indicate that the morphological changes described in both beaches are related not only to wave conditions but also to the geological setting. In natural beaches, changes in morphology are driven by dynamic forces, primarily waves, operating on a particular volume of sediment within the boundaries of the surrounding geological framework and sea level position [55]. The geological setting is described as a secondary factor controlling beach morphodynamics [56].

On the other hand, Patos Beach is influenced by the coastline orientation and its geological setting as semi-exposed sheltered beach with an orientation towards the Atlan-tic fetch. The morphology of sheltered beaches varies widely depending on coastal setting, i.e., their location inside the estuary or bay [28,32,57]. The primary southwest-northeast orientation of the Ria and the presence of the Cíes Islands (Figure 1) at the mouth generate different degrees of wave exposure and beach characteristics [32]. Numerical simulations regarding the presence of Cíes Islands show that these islands reduce significant wave heights in the outer sector of the ria, where Patos Beach is located [58]. The wave regime in Patos is primarily controlled by northwesterly waves, but within the ria, the contributions of swell and wind sea may vary, influenced by factors such as remotely generated swell, the shelf and inner Ria winds, and the geomorphology of the Ria itself [59]. The presence of headlands and rocky outcrops in the shoreface which are identified by our bathymetric survey can also influence morphodynamics affecting Patos. In fact, [30] demonstrated that the beach dynamics and cross-shore transport trend diminish towards the south, coincident with shadow zones near the headlands [28]. Previous research demonstrate the accumulation of sand in the subtidal and intertidal zones of the beach at the short-term [54]. Furthermore, pocket beaches with an oblique wave approach have significant dynamics with consequent. Although we cannot identify beach rotation, some case studies [60,61], describe a triggering mechanism (e.g., storms or groups of storms) that results in a short-term (days to weeks) rotation [62]. A more extensive monitoring or modeling of the shoreline at higher spatial and temporal scales would be needed to conduct a comprehensive analysis of the beach rotation processes [63,64].

This configuration results in a morphodynamic behavior with relatively stable equilibrium, common for a semi-sheltered beach. According to [65], the depth of closure allows to classify the embayments as closed, semi-closed, or open. In the case of Patos beach, the depth of closure in winter 2018/19 exceeds 8 m deep (Figure 6), which is shallower than the isobathic line connecting the headlands. As a result, Patos may correspond to a closed embayment. This study also highlights the sediment budget between the aerial and submerged beach during winter, indicating almost a balanced equilibrium between erosion and accretion. Berm erosion is generally linked to the pre-storm beach volume and wave energy. In Patos Beach, the influence of the geological setting reduces wave energy in the nearshore, affecting the sedimentary dynamics during winter. The geomorphological context as an embayed setting may confer a specific ability to retain sediments despite energetic winter conditions.

In Mira, the sedimentary dynamics are more pronounced, as evidenced by the greater volumetric changes in the beach profiles (up to -170 m^3/m) and the volume involved in berm erosion (Figure 7). Mira Beach reveals sediment transport exchanges in both the cross-shore and long-shore directions, with a strong longshore component. In addition, a slightly positive sediment balance has been obtained for the entire nearshore area during the winter, although some errors in the bathymetric method may affect this sediment budget result.

Regarding the subaerial beach and dune system, previous research has observed coastline retreat and dune erosion, indicating a long-term progressive erosional trend at open Mira Beach [34,38,66]. This study confirms the erosional trend in the subaerial beach for the winter timescale. This stretch has been identified as an erosion hotspot, and to mitigate coastal erosion in this sector, artificial structures and groins have been constructed [41]. During the winter 2018/19, the sediment budget in the subaerial beach is negative, and beach profile trends indicate an erosive pattern with up to -44 m of shoreline migration. In comparison to Patos, in Mira, longshore transport plays a more significant role [39]. The presence of beach cusps [34] and sandbars in the nearshore (Figure 7) that migrate southwards at the end of the analyzed period confirms the longshore dynamics and variability in this coastal area.

New technologies and precision survey methods, such as satellite and unmanned aerial vehicles (UAV), can rapidly improve our understanding of process-response dynamics [67],

especially on medium-to-long-term timescales [68]. However, it remains a major challenge to obtain adequate data collection to study morphological changes in shallow submerged areas where remote sensing is still under development [69].

However, high-resolution coastal monitoring can provide fundamental data for future coastal analysis and modeling. Coastal management of beaches and dunes is critical for reducing erosion on high-energy sandy coasts. The differences in beach responses reflect important morphologic distinctions driven by hydrodynamic processes and geological framework features. The erosion trend and morphological evolution on the embayed and open beaches may determine the success of beach nourishment projects and coastal zone management.

Although the importance of coastal monitoring is well known, it is very common that coastal studies and management projects are carried out without an adequate knowledge of the submerged zone. Patos and Mira beaches are both anthropized coastal areas. Patos has been urbanized in the backshore with a promenade and nearby buildings. In Mira, even though it preserves part of its natural dune, it has been modified by dune nourishments that have intensified in recent years [34,41]. It is not possible to evaluate the morphological evolution as if they were natural beaches. This aspect is important and adds complexity to determining the future of these sedimentary environments. The missing bathymetry data limits the morphodynamic analysis, since the nearshore bars location affect the nearshore wave propagation on the barred coastal stretch of Mira Beach, and consequently the wave impact on the dunes [34,47]. Conventional vessel-based bathymetric measurements are complex tasks to perform with the required frequency, in particular on high-energy coasts. This is particularly important on the Portuguese coast evolution, where erosion hotspots have been identified, and coastal monitoring can determine the future of many communities at risk [39,41,66,70].

The beaches monitored in this study exhibited clear differences with Patos Beach, showing gradual erosion in winter, while Mira Beach showed significant changes in a few days (Table 5). Therefore, the spatial and temporal monitoring scales should be shorter at Mira Beach to obtain more accurate results, either to quantify changes or to use these indicators as a basis for shoreline evolution or storm impact models. By collecting data over an extended period, coastal monitoring programs can identify long-term erosion trends and assess the impacts of climate change and sea-level rise.

6. Conclusions

Over the last decade, the alternating winters and summers impose a clear seasonal wave pattern in the northwest Iberian region, with weaker waves from May to October. The 2013/14 winter is identified as the most severe, with the highest number of storms and storm clusters. The 2018/19 winter also represents one of the most energetic periods in the last 10 years. Both analyzed beaches experienced similar wave forcing in winter.

The embayed Patos Beach displays a more gradual and uniform response, with lower dynamics and a more stable morphology. The winter storms lead to the removal of sediments from the subaerial beach, causing berm erosion and shoreline retreat (i.e., landward. The surf zone of the beach developed a sandbar. The open Mira Beach shows significant morphological variations, with strong dynamics in the submerged zone and notable volumetric changes. The winter storms redistribute sediment along the coastline, generating significant changes on the beach topography and particularly modifying the submerged sand bars.

Differences in morphodynamic response are attributed not only to wave conditions but also to the geological context. Patos, a semi-exposed beach inside the Vigo ria and protected by Cíes Islands, demonstrates a relatively stable equilibrium, with coastline orientation and the presence of islands reducing wave heights. In contrast, Mira, an open beach, undergoes more pronounced sedimentary dynamics, with evident volumetric changes due to significant longshore and cross-shore sediment transport.

Both beaches have been altered by human intervention, with minor modifications in Patos Beach (a promenade over the dunes), while Mira Beach present nearby coastal structures and nourishment measures. Urbanization and anthropogenic modifications add complexity to assessing the future evolution of these beaches.

Combined high-resolution monitoring of the subaerial and submerged coastal areas is crucial for understanding morphological dynamics and modeling the impacts of changing environmental conditions. Differences in beach responses underscore the importance of site-specific investigations in coastal management and beach nourishment projects.

Supplementary Materials: The following supporting information can be downloaded at https://www.mdpi.com/article/10.3390/jmse12010168/s1. Figure S1: Morphological changes (difference in m, black lines) in four additional cross-shore profiles from Mira Beach between the pre-winter (blue line, September 2018) and post-winter (red lines, June 2019) topographies (elevation in m above mean sea level).

Author Contributions: Conceptualization, Á.F.-B. and T.A.; methodology, Á.F.-B., T.A., C.C.F., P.A.S. and J.A.-C.; validation, Á.F.-B., T.A. and C.C.F.; formal analysis, Á.F.-B., T.A., C.C.F., P.A.S. and J.A.-C.; investigation, Á.F.-B., T.A., C.C.F., P.A.S. and J.A.-C.; resources, Á.F.-B., T.A., C.C.F. and L.L.-O.; data curation, Á.F.-B., T.A., C.C.F. and J.A.-C.; writing—original draft preparation, Á.F.-B., T.A. and J.A.-C.; writing—review and editing, Á.F.-B., T.A., C.C.F., P.A.S., J.G., A.M.B. and J.A.-C.; visualization, Á.F.-B., T.A., C.C.F. and J.A.-C.; supervision, Á.F.-B. All authors have read and agreed to the published version of the manuscript.

Funding: Thanks are due to ED481D2019/028 postdoc project awarded by Xunta de Galicia (Spain) and to FCT/MCTES for the financial support of CESAM (UIDP/50017/2020 + UIDB/50017/2020+ LA/P/0094/2020), through national funds. J.A.-C. thanks the grant "Ayudas para la Recualificación del Sistema Universitario Español" (ref. CA2/RSUE/2021-00418) of the Spanish Ministry of Universities.

Institutional Review Board Statement: Not applicable.

Informed Consent Statement: Not applicable.

Data Availability Statement: The data presented in this study are available on request from the corresponding author.

Acknowledgments: Special thanks are given to Umberto Andriolo, Kais Mohamed Falcon and all colleagues who have contributed to field surveys. The authors would like to thank the four anonymous reviewers for all useful and helpful comments on our manuscript.

Conflicts of Interest: The authors declare no conflict of interest.

References

1. Masselink, G.; Pattiaratchi, C.B. Seasonal changes in beach morphology along the sheltered coastline of Perth, Western Australia. *Mar. Geol.* **2001**, *172*, 243–263. [CrossRef]
2. Wright, L.D.; Short, A.D. Morphodynamic variability of surf zones and beaches: A synthesis. *Mar. Geol.* **1984**, *56*, 93–118. [CrossRef]
3. Andriolo, U.; Gonçalves, G. Is coastal erosion a source of marine litter pollution? Evidence of coastal dunes being a reservoir of plastics. *Mar. Pollut. Bull.* **2022**, *174*, 113307. [CrossRef] [PubMed]
4. Barnard, P.L.; Short, A.D.; Harley, M.D.; Splinter, K.D.; Vitousek, S.; Turner, I.L.; Allan, J.; Banno, M.; Bryan, K.R.; Doria, A.; et al. Coastal vulnerability across the Pacific dominated by El Niño/Southern Oscillation. *Nat. Geosci.* **2015**, *8*, 801–807. [CrossRef]
5. Jackson, N.L.; Nordstrom, K.F.; Feagin, R.A.; Smith, W.K. Coastal geomorphology and restoration. *Geomorphology* **2013**, *199*, 1–7. [CrossRef]
6. Román-Rivera, M.A.; Ellis, J.T. A synthetic review of remote sensing applications to detect nearshore bars. *Mar. Geol.* **2019**, *408*, 144–153. [CrossRef]
7. Garnier, E.; Ciavola, P.; Spencer, T.; Ferreira, O.; Armaroli, C.; McIvor, A. Historical analysis of storm events: Case studies in France, England, Portugal and Italy. *Coast. Eng.* **2018**, *134*, 10–23. [CrossRef]
8. Karunarathna, H.; Pender, D.; Ranasinghe, R.; Short, A.D.; Reeve, D.E. The effects of storm clustering on beach profile variability. *Mar. Geol.* **2014**, *348*, 103–112. [CrossRef]
9. Loureiro, C.; Ferreira, Ó.; Cooper, J.A.G. Extreme erosion on high-energy embayed beaches: Influence of megarips and storm grouping. *Geomorphology* **2012**, *139–140*, 155–171. [CrossRef]

10. Phillips, M.S.; Harley, M.D.; Turner, I.L.; Splinter, K.D.; Cox, R.J. Shoreline recovery on wave-dominated sandy coastlines: The role of sandbar morphodynamics and nearshore wave parameters. *Mar. Geol.* **2017**, *385*, 146–159. [CrossRef]
11. Senechal, N.; Coco, G.; Castelle, B.; Marieu, V. Storm impact on the seasonal shoreline dynamics of a meso- to macrotidal open sandy beach (Biscarrosse, France). *Geomorphology* **2015**, *228*, 448–461. [CrossRef]
12. Burvingt, O.; Masselink, G.; Russell, P.; Scott, T. Classification of beach response to extreme storms. *Geomorphology* **2017**, *295*, 722–737. [CrossRef]
13. Vousdoukas, M.I.; Mentaschi, L.; Feyen, L.; Voukouvalas, E. Earth's Future Extreme sea levels on the rise along Europe's coasts Earth's Future. *Earth's Futur.* **2017**, *5*, 304–323. [CrossRef]
14. Short, A.D. Australian beach systems: Are they at risk to climate change? *Ocean Coast. Manag.* **2022**, *224*, 106180. [CrossRef]
15. Woolf, D.K.; Challenor, P.G.; Cotton, P.D. Variability and predictability of the North Atlantic wave climate. *J. Geophys. Res. Ocean.* **2002**, *107*, 9-1–9-14. [CrossRef]
16. Lozano, I.; Devoy, R.J.N.; May, W.; Andersen, U. Storminess and vulnerability along the Atlantic coastlines of Europe: Analysis of storm records and of a greenhouse gases induced climate scenario. *Mar. Geol.* **2004**, *210*, 205–225. [CrossRef]
17. Burvingt, O.; Castelle, B. Storm response and multi-annual recovery of eight coastal dunes spread along the Atlantic coast of Europe. *Geomorphology* **2023**, *435*, 108735. [CrossRef]
18. Castelle, B.; Dodet, G.; Masselink, G.; Scott, T. A new climate index controlling winter wave activity along the Atlantic coast of Europe: The West Europe Pressure Anomaly. *Geophys. Res. Lett.* **2017**, *44*, 1384–1392. [CrossRef]
19. Bertin, X.; Prouteau, E.; Letetrel, C. A significant increase in wave height in the North Atlantic Ocean over the 20th century. *Glob. Planet. Chang.* **2013**, *106*, 77–83. [CrossRef]
20. Castelle, B.; Dodet, G.; Masselink, G.; Scott, T. Increased Winter-Mean Wave Height, Variability, and Periodicity in the Northeast Atlantic Over 1949–2017. *Geophys. Res. Lett.* **2018**, *45*, 3586–3596. [CrossRef]
21. Ferreira, Ó.; Plomaritis, T.A.; Costas, S. Process-based indicators to assess storm induced coastal hazards. *Earth-Sci. Rev.* **2017**, *173*, 159–167. [CrossRef]
22. Masselink, G.; Van Heteren, S. Response of wave-dominated and mixed-energy barriers to storms. *Mar. Geol.* **2014**, *352*, 321–347. [CrossRef]
23. Roberts, T.M.; Wang, P.; Puleo, J.A. Storm-driven cyclic beach morphodynamics of a mixed sand and gravel beach along the Mid-Atlantic Coast, USA. *Mar. Geol.* **2013**, *346*, 403–421. [CrossRef]
24. Eichentopf, S.; Alsina, J.M.; Christou, M.; Kuriyama, Y. Storm sequencing and beach profile variability at Hasaki, Japan. *Mar. Geol.* **2020**, *424*, 106153. [CrossRef]
25. Ciavola, P.; Ferreira, O.; Haerens, P.; Van Koningsveld, M.; Armaroli, C.; Lequeux, Q. Storm impacts along European coastlines. Part 1: The joint effort of the MICORE and ConHaz Projects. *Environ. Sci. Policy* **2011**, *14*, 912–923. [CrossRef]
26. Dehouck, A.; Dupuis, H.; Sénéchal, N. Pocket beach hydrodynamics: The example of four macrotidal beaches, Brittany, France. *Mar. Geol.* **2009**, *266*, 1–17. [CrossRef]
27. Gallop, S.L.; Vila-Concejo, A.; Fellowes, T.E.; Harley, M.D.; Rahbani, M.; Largier, J.L. Wave direction shift triggered severe erosion of beaches in estuaries and bays with limited post-storm recovery. *Earth Surf. Process. Landf.* **2020**, *45*, 3854–3868. [CrossRef]
28. Fellowes, T.E.; Vila-Concejo, A.; Gallop, S.L.; Harley, M.D.; Short, A.D. Wave shadow zones as a primary control of storm erosion and recovery on embayed beaches. *Geomorphology* **2022**, *399*, 108072. [CrossRef]
29. Da Fontoura Klein, A.H.; Benedet Filho, L.; Schumacher, D.H. Short-term beach rotation processes in distinct headland bay beach systems. *J. Coast. Res.* **2002**, *18*, 442–458.
30. Rey, S.; Alejo, I.; Alcántara-Carrió, J.; Vilas, F. Influence of Boundary Conditions on Morphodynamics and Sedimentology of Patos Beach (Ría de Vigo, Nw of Spain). In *Littoral 2002, The Changing Coast*; EUROCOAST/EUCC: Porto, Portugal, 2002; pp. 277–280.
31. Vilas, F.; Bernabeu, A.M.; Méndez, G. Sediment distribution pattern in the Rias Baixas (NW Spain): Main facies and hydrodynamic dependence. *J. Mar. Syst.* **2005**, *54*, 261–276. [CrossRef]
32. Bernabeu, A.M.; Lersundi-Kanpistegi, A.V.; Vilas, F. Gradation from oceanic to estuarine beaches in a ría environment: A case study in the Ría de Vigo. *Estuar. Coast. Shelf Sci.* **2012**, *102–103*, 60–69. [CrossRef]
33. Rey, S.; Alejo, I.; Alonso, I.; Alcantara-Carrio, J. Field determination of sediment transport patterns: A case study from Patos Beach (Northwest Spain). *J. Coast. Res.* **2006**, *2004*, 607–610.
34. Fontán-Bouzas, Á.; Andriolo, U.; Silva, P.A.; Baptista, P. Wave Impact Analysis on a Beach-Dune System to Support Coastal Management and Nourishment Works: The Showcase of Mira, Portugal. *Front. Mar. Sci.* **2022**, *9*, 861569. [CrossRef]
35. Silva, R.; Baptista, P.; Veloso-Gomes, F.; Coelho, C.; Taveira-Pinto, F. Sediment grain size variation on a coastal stretch facing the North Atlantic (NW Portugal). *J. Coast. Res.* **2009**, *I*, 762–766.
36. Stronkhorst, J.; Huisman, B.; Giardino, A.; Santinelli, G.; Santos, F.D. Sand nourishment strategies to mitigate coastal erosion and sea level rise at the coasts of Holland (The Netherlands) and Aveiro (Portugal) in the 21st century. *Ocean Coast. Manag.* **2018**, *156*, 266–276. [CrossRef]
37. Fernández-Fernández, S.; Ferreira, C.C.; Silva, P.A.; Baptista, P.; Romão, S.; Fontán-Bouzas, Á.; Abreu, T.; Bertin, X. Assessment of Dredging Scenarios for a Tidal Inlet in a High-Energy Coast. *J. Mar. Sci. Eng.* **2019**, *7*, 395. [CrossRef]
38. Baptista, P.; Coelho, C.; Pereira, C.; Bernardes, C.; Veloso-Gomes, F. Beach morphology and shoreline evolution: Monitoring and modelling medium-term responses (Portuguese NW coast study site). *Coast. Eng.* **2014**, *84*, 23–37. [CrossRef]

39. López-Olmedilla, L.; Almeida, L.P.; de Figueiredo, S.A.; Fontán-Bouzas, Á.; Silva, P.A.; Alcántara-Carrió, J. Effect of alongshore sediment supply gradients on projected shoreline position under sea-level rise (northwestern Portuguese coast). *Estuar. Coast. Shelf Sci.* **2022**, *271*, 107876. [CrossRef]
40. Marinho, B.; Coelho, C.; Larson, M.; Hanson, H. Short- and long-term responses of nourishments: Barra-Vagueira coastal stretch, Portugal. *J. Coast. Conserv.* **2018**, *22*, 475–489. [CrossRef]
41. Pinto, C.A.; Silveira, T.M.; Teixeira, S.B. Beach nourishment practice in mainland Portugal (1950–2017): Overview and retrospective. *Ocean Coast. Manag.* **2020**, *192*, 105211. [CrossRef]
42. Antunes, C.; Taborda, R. Sea level at cascais tide gauge: Data, analysis and results. *J. Coast. Res.* **2009**, *56*, 218–222.
43. Pilar, P.; Soares, C.G.; Carretero, J.C. 44-year wave hindcast for the North East Atlantic European coast. *Coast. Eng.* **2008**, *55*, 861–871. [CrossRef]
44. Dolan, R.; Davis, R. Coastal Storm Hazards. *J. Coast. Res.* **1994**, *12*, 103–114.
45. Biausque, M.; Senechal, N. Seasonal morphological response of an open sandy beach to winter wave conditions: The example of Biscarrosse beach, SW France. *Geomorphology* **2019**, *332*, 157–169. [CrossRef]
46. Castelle, B.; Bujan, S.; Ferreira, S.; Dodet, G. Foredune morphological changes and beach recovery from the extreme 2013/2014 winter at a high-energy sandy coast. *Mar. Geol.* **2017**, *385*, 41–55. [CrossRef]
47. Castelle, B.; Marieu, V.; Bujan, S.; Splinter, K.D.; Robinet, A.; Sénéchal, N.; Ferreira, S. Impact of the winter 2013-2014 series of severe Western Europe storms on a double-barred sandy coast: Beach and dune erosion and megacusp embayments. *Geomorphology* **2015**, *238*, 135–148. [CrossRef]
48. Scott, T.; Masselink, G.; O'Hare, T.; Saulter, A.; Poate, T.; Russell, P.; Davidson, M.; Conley, D. The extreme 2013/2014 winter storms: Beach recovery along the southwest coast of England. *Mar. Geol.* **2016**, *382*, 224–241. [CrossRef]
49. Flor-Blanco, G.; Alcántara-Carrió, J.; Jackson, D.W.T.; Flor, G.; Flores-Soriano, C. Coastal erosion in NW Spain: Recent patterns under extreme storm wave events. *Geomorphology* **2021**, *387*, 107767. [CrossRef]
50. Oliveira, T.C.; Cagnin, E.; Silva, P.A. Wind-waves in the coast of mainland Portugal induced by post-tropical storms. *Ocean Eng.* **2020**, *217*, 108020. [CrossRef]
51. Gomes, M.P.; Santos, L.; Pinho, J.L.; Do Carmo, J.S.A. Hazard assessment of storm events for the portuguese northern coast. *Geosciences* **2018**, *8*, 178. [CrossRef]
52. Antunes, C.; Rocha, C.; Catita, C. Coastal flood assessment due to sea level rise and extreme storm events: A case study of the atlantic coast of Portugal's mainland. *Geosciences* **2019**, *9*, 6–8. [CrossRef]
53. Masselink, G.; Castelle, B.; Scott, T.; Konstantinou, A. Role of Atmospheric Indices in Describing Shoreline Variability Along the Atlantic Coast of Europe. *Geophys. Res. Lett.* **2023**, *50*, e2023GL106019. [CrossRef]
54. Ferreira, C.C.; Silva, P.A.; Bernabeu, A.M.; Fontán-Bouzas, Á.; Fernández-Fernández, S.; Abreu, T. Tracking fluorescent tracer to monitor grain size-selective dispersion in subtidal zone: Patos Beach case study (NW Iberian Peninsula). *Reg. Stud. Mar. Sci.* **2024**, *69*, 103303. [CrossRef]
55. Cooper, J.A.G.; Pilkey, O.H. Sea-level rise and shoreline retreat: Time to abandon the Bruun Rule. *Glob. Planet. Change* **2004**, *43*, 157–171. [CrossRef]
56. Jackson, D.W.T.; Cooper, J.A.G.; Del Rio, L. Geological control of beach morphodynamic state. *Mar. Geol.* **2005**, *216*, 297–314. [CrossRef]
57. Gallop, S.L.; Kennedy, D.M.; Loureiro, C.; Naylor, L.A.; Muñoz-Pérez, J.J.; Jackson, D.W.T.; Fellowes, T.E. Geologically controlled sandy beaches: Their geomorphology, morphodynamics and classification. *Sci. Total Environ.* **2020**, *731*, 139123. [CrossRef] [PubMed]
58. Fontán-Bouzas, A.; Ferreira, C.C.; Abreu, T.; Bernabeu, A.; Silva, P.A.; Alcántara-Carrió, J.; Portz, L.; Manzolli, R. The role of the Cíes Islands on the wave regime and morphodynamics of the pocket beaches (Vigo Ria, Northwestern Iberian Peninsula). In Proceedings of the XI Coastal Geomorphology Conference, Santiago de Compostela, Spain, 27–29 July 2022; pp. 85–89.
59. Villacieros-Robineau, N.; Gilcoto, M.; Pardo, P.C.; Barton, E.D. Wave regime and wave-current coupling in an upwelling–driven bay: Seasonal and inter-annual variability. *J. Geophys. Res. Ocean.* **2021**, *126*, e2021JC017540. [CrossRef]
60. Harley, M.D.; Turner, I.L.; Short, A.D. New insights into embayed beach rotation: The importance of wave exposure and cross-shore processes. *J. Geophys. Res. Earth Surf.* **2015**, *120*, 1470–1484. [CrossRef]
61. Ojeda, E.; Guillén, J. Shoreline dynamics and beach rotation of artificial embayed beaches. *Mar. Geol.* **2008**, *253*, 51–62. [CrossRef]
62. Loureiro, C.; Ferreira, Ó. *Mechanisms and Timescales of Beach Rotation*; Elsevier Ltd.: Amsterdam, The Netherlands, 2020; ISBN 9780081029275.
63. Castelle, B.; Robinet, A.; Idier, D.; D'Anna, M. Modelling of embayed beach equilibrium planform and rotation signal. *Geomorphology* **2020**, *369*, 107367. [CrossRef]
64. Fellowes, T.E.; Vila-Concejo, A.; Gallop, S.L. Morphometric classification of swell-dominated embayed beaches. *Mar. Geol.* **2019**, *411*, 78–87. [CrossRef]
65. Bowman, D.; Rosas, V.; Pranzini, E. Pocket beaches of Elba Island (Italy)—Planview geometry, depth ofclosure and sediment dispersal. *Estuar. Coast. Shelf Sci.* **2014**, *138*, 37–46. [CrossRef]
66. Ponte Lira, C.; Silva, A.N.; Taborda, R.; De Andrade, C.F. Coastline evolution of Portuguese low-lying sandy coast in the last 50 years: An integrated approach. *Earth Syst. Sci. Data* **2016**, *8*, 265–278. [CrossRef]

67. Andriolo, U.; Gonçalves, G.; Sobral, P.; Fontán-Bouzas, Á.; Bessa, F. Beach-dune morphodynamics and marine macro-litter abundance: An integrated approach with Unmanned Aerial System. *Sci. Total Environ.* **2020**, *749*, 141474. [CrossRef] [PubMed]
68. Vitousek, S.; Buscombe, D.; Vos, K.; Barnard, P.L.; Ritchie, A.C.; Warrick, J.A. The future of coastal monitoring through satellite remote sensing. In *Cambridge Prisms: Coastal Futures*; Cambridge University Press: Cambridge, UK, 2022; Volume 1.
69. Santos, D.; Fernández-Fernández, S.; Abreu, T.; Silva, P.A.; Baptista, P. Retrieval of nearshore bathymetry from Sentinel-1 SAR data in high energetic wave coasts: The Portuguese case study. *Remote Sens. Appl. Soc. Environ.* **2022**, *25*, 100674. [CrossRef]
70. Mendes, D.; Pais-Barbosa, J.; Baptista, P.; Silva, P.A.; Bernardes, C.; Pinto, C. Beach Response to a Shoreface Nourishment (Aveiro, Portugal). *J. Mar. Sci. Eng.* **2021**, *9*, 1112. [CrossRef]